We are IntechOpen,
the world's leading publisher of
Open Access books
Built by scientists, for scientists

6,900
Open access books available

186,000
International authors and editors

200M
Downloads

Our authors are among the

154
Countries delivered to

TOP 1%
most cited scientists

12.2%
Contributors from top 500 universities

CLARIVATE ANALYTICS
BOOK CITATION INDEX
INDEXED

WEB OF SCIENCE™

Selection of our books indexed in the Book Citation Index
in Web of Science™ Core Collection (BKCI)

Interested in publishing with us?
Contact book.department@intechopen.com

Numbers displayed above are based on latest data collected.
For more information visit www.intechopen.com

Chapter

Physics of Nanostructure Design for Infrared Detectors

Nibir Kumar Dhar, Samiran Ganguly and Srini Krishnamurthy

Abstract

Infrared detectors and focal plane array technologies are becoming ubiquitous in military, but are limited in the commercial sectors. The widespread commercial use of this technology is lacking because of the high cost and large size, weight and power. Most of these detectors require cryogenic cooling to minimize thermally generated dark currents, causing the size, weight, power and cost to increase significantly. Approaches using very thin detector design can minimize thermally generated dark current, but at a cost of lower absorption efficiency. There are emerging technologies in nanostructured material designs such as metasurfaces that can allow for increased photon absorption in a thin detector architecture. Ultra-thin and low-dimensional absorber materials may also provide unique engineering opportunities in detector design. This chapter discusses the physics and opportunities to increase the operating temperature using such techniques.

Keywords: infrared detectors, nanostructure, metasurfaces, plasmonics, detector noise, dark current, absorption, thin absorber, photon trap

1. Introduction

Infrared (IR) detectors and focal plane array technologies (FPA) have proven to be at the heart of many defense and commercial applications. Most of these detectors require cryogenic cooling to minimize thermally generated dark current, causing the size, weight, power and cost (SWaP-C) to increase significantly. The objective of this chapter is to discuss physics and development of new approaches in nanostructure engineering of light matter interaction to enhance photon field absorption in very thin infrared absorbing layers, thereby significantly reduce thermally generated noise, thus paving a path to higher operating temperature and eliminating bulky and costly cryogenic coolers. Breakthroughs are necessary in materials design to considerably reduce the detector noise caused by the surface leakage and dark current to enable high operating temperature. The device architecture must be commensurate with improved quantum efficiency and increased lifetime, ideally being only background shot noise limited. This however cannot be accomplished by merely improving the material quality alone. Achieving extremely low dark currents at higher temperature using nanostructured thin absorption layers will lead to practical infrared detector technology that can have wide spread applications.

Since the early 50s, there has been considerable progress towards the materials development and device design innovations. In particular, significant advances have been made during the past couple of decades in the bandgap engineering of various compound semiconductors that has led to new and emerging detector architectures. Advances in optoelectronics related materials science, such as metamaterials, nanostructures and 2D material designs have opened doors for new approaches to apply device design methodologies, which are expected to offer enhanced performance at higher operating temperature and lower cost products in a wide range of applications.

This chapter discusses advancements in the detector technologies and presents physics of emerging device architectures. The chapter introduces the basics of infrared detection physics and various detector figure of merit (FOM). Advances in pixel scaling, junction formation, materials growth, bandstructure design and processing technologies have matured substantially to make an impact towards higher operating temperature detectors [1]. The concepts presented here are informational in nature for students interested in infrared detector technology. The central ideas discussed are the opportunities to use thin detector designs to reduce thermally generated dark current and increasing radiation absorption techniques. Thus achieving lower SWaP-C.

2. Detector characterization parameters

IR detectors can be categorized as being either a quantum or thermal device. In a quantum detector, electromagnetic radiation absorbed in a semiconductor material generates electron-hole pairs, which are sensed by an electronic readout circuit (ROIC). In a thermal detector, on the other hand, the incident IR photons are absorbed by a thermally isolated detector element, resulting in an increase in the temperature of the element. The temperature is sensed by monitoring an electrical parameter such as resistivity or capacitance. In this chapter we are primarily concerned with quantum detectors.

Due to the various mechanisms used by detectors to convert optical to electrical signals, several FOM are used to characterize their performance. The output of the detector consists of its response signal to the incident radiation and random noise fluctuations. One such FOM is the Responsivity (R) of the detector, defined as the ratio of the root mean squared (RMS) value of the signal voltage (V_s) or output current to the RMS input radiation power (ϕ) incident on the detector. The responsivity is given as:

$$R_v(\lambda, f) = \frac{V_s}{\phi(\lambda)}; R_i(\lambda, f) = \frac{I_s}{\phi(\lambda)} \qquad (1)$$

The spectral current responsivity can also be written in terms of quantum efficiency as:

$$R_i(\lambda, f) = \frac{\lambda \eta}{hc} qg \qquad (2)$$

Where, λ is the photon wavelength, η is the quantum efficiency (QE) (more on QE in Section 4), h is the Plank's constant, c is the speed of light, q is the electronic charge and g is the gain. For photovoltaic (p/n junction) detectors $g = 1$.

The responsivity is usually a function of the bias voltage, the operating electrical frequency, and the wavelength. An important parameter typically used in infrared

detectors is the Noise Equivalent Power (NEP). It is the minimum incident radiant power on the detector required to produce a SNR of unity. Therefore, it can be expressed as:

$$\text{NEP} = \frac{V_n}{R_v} = \frac{I_n}{R_i} \tag{3}$$

NEP is usually measured for a fixed reference bandwidth. The NEP is typically proportional to the square root of the detector signal, which is proportional to the detector area of optical collection Ad. An important factor in detector operation is the detectivity D, which is the reciprocal of NEP. It is the signal-to-noise ratio. There are multiple approaches to characterize this FOM, a useful one is the specific or normalized detectivity, D^* given by:

$$D^* = D\left(\sqrt{\delta f A d}\right) = \frac{\sqrt{\delta f A d}}{NEP} \tag{4}$$

Or

$$D^* = \frac{I_{signal}}{I_{noise}} \frac{\sqrt{\delta f A d}}{P_{opt}} \tag{5}$$

Where, $I_{signal} = I_{lit} - I_{dark}$ and I_{lit} is the photocurrent, δf is the bandwidth of the measurement, Ad is the detector optical area, P_{opt} is the optical power (ϕ_λ) incident on the detector, and I_{noise} is the RMS noise current. This noise current depends on the dark current I_{dark} and its exact formulation depends on the type of noise dominant in the detector. These noises are primarily of the following four kinds:

a. Thermal or Johnson noise which occurs due to thermal agitation of the electrons in the detector material and can be controlled by cryogenic approaches and is given by $I^2_{noise} = 4kT/R$ where R is the dark resistance.

b. Flicker or 1/f noise which occurs due to stochasticity of the time of arrival of electrons through the detector film to the contact terminals and is given by $I^2_{noise} = \alpha_H/nf$ where α_H is Hooge's constant, n is the number of transporting carriers, and f is the measurement frequency. It can be seen that this noise is lower at higher measurement frequencies, and is controlled by high frequency measurements using modulated read signal in kHz ranges, or optical choppers that provide an additional means of reducing the flicker noise.

c. Shot noise occurs due to stochasticity in counting statistics of the number of carriers in the detector material and is given by $I^2_{noise} = 2q|I|$.

d. Recombination-Generation noise that arises due to stochasticity of recombination and generation processes of electrons and holes and is given as $I^2_{noise} \propto 4I^2/n\left(1 + 4\pi^2 f^2 \tau^2\right)$. This can be improved by material processing and detector design to reduce recombination rate.

It is clear from the above discussion that the performance of the detector is heavily impacted by the dark current. Lower is the dark current, higher is the relative signal and lower is the noise. *Therefore, dark current reduction without sacrificing photogeneration is the central goal of detector design and engineering*.

3. Dark current vs. temperature

The ultimate in detector performance is achieved when the noise generated by the background (scene) flux is greater than any thermally generated noise within the detector (for more information see Ref. [2]). Such condition is termed as background Limited Performance or BLIP. It can be seen that the bigger component of noise inherent in the detector is the dark current. It is the output current when no background flux is incident on the detector and depends strongly on the detector temperature. The dark current increases with temperature since the carrier thermal energy KT increases with temperature. When the carrier thermal energy is equal to or greater than the bandgap (E_g) energy, more thermally generated carriers are promoted to the conduction band giving rise to dark current. It is this reason; quantum detectors need to be cooled to a temperature that minimizes the dark current. However, this requires cooling to cryogenic temperature where large coolers are used. This is an inherent problem because it increases the size, weight, power and cost.

The dark current with respect to temperature can be defined as an Arrhenius equation [3]:

$$I_{dark}(T) = A_e J_0 \mathrm{Texp}\left(\frac{-E_a}{K_B T}\right) \tag{6}$$

Where A_e is the electronic area of the detector, J_0 is a constant that depends on the detector absorber materials properties, K_B is the Boltzmann constant, T is the detector temperature and E_a is the activation energy to promote a carrier into the conduction band. This equation clearly illustrates how dark current increases with temperature. The BLIP condition is achieved at a temperature (T_{BLIP}) where photocurrent becomes equal to the dark current.

4. Fundamental photon detector action: absorption, generation, detection

Photodetectors can be built in a variety of device configurations [4]. The major ones include a light dependent conductor (photoconductor), light dependent diode (photodiode, avalanche photo-diode), photovoltaic (such as solar cell), or thermal detector/bolometer (Seebeck effect detectors). At the most fundamental level, all these devices depend on the excitation of matter particles by transferring incident photon energy into the absorber material. In the case of a thermal detector, the excited matter particles are phonons and electrons, in the case of a photovoltaic or photoconductive detector, it is an electron-hole pair also called excitons, and in certain cases it is plasmons acting as an intermediary between the electrons and photons.

It is obvious that the photodetector action depends on the transduction efficiency of the absorbed photons (light) into a detector particle species, primarily an electron (matter) and its subsequent electrical readout. This efficiency is called the internal quantum efficiency (IQE). In most high-quality detectors, this approaches unity, though it is possible to obtain higher than one IQE if the material bandstructure can be engineered to emit more than one electron per absorbed photon, which typically needs special quantum engineered bandstructures, since the electron relaxation post-generation must be "direct" or radiative. External quantum efficiency (EQE) captures the effect of light absorption within this approach, i.e. EQE = Absorption × IQE.

EQE is a function dependent principally on three factors: photon wavelength, detector temperature, and absorption efficiency. We illustrate this using an example as follows. In Ref. [5] we developed a quantum mechanical model of IQE in poly-crystalline PbSe mid-wave IR detectors. This formulation is developed on the lines of the Shockley-Quiesser approach [6]. In this approach the photons of energies larger than the material bandgap first thermalizes to the band edge and then creates a photo-generated carrier. We modeled the absorption efficiency using the classic Moss model [7] which considers non-uniformity of photon absorption in film thickness direction, x, film reflectivity r, and effective absorption coefficient α, and is given by:

$$\kappa(x) = \frac{(1-r)(1-e^{\alpha x})}{1-re^{\alpha x}} \tag{7}$$

The IQE is given by excitation of matter particle modes. In the same example the carrier generation is given as:

$$\eta_{IQE}(\lambda, T) = \frac{E_g(T)\int_0^\infty D(E,\lambda)N(E,\lambda)\zeta(E,T)dE}{\int_0^\infty ED(E,\lambda)N(E,\lambda)dE} \tag{8}$$

Where E_g is the bandgap (a function of detector temperature, T), D, N are photon density of states and occupancy function, which itself is a function of phonon spectra (and hence a function of wavelength λ), and a band edge disorder function ζ which accounts for Urbach tails [8] into the bandgap (again dependent on T). The overall EQE is then given by:

$$\eta_{EQE}(\lambda, T, x) = \eta_{IQE}(\lambda, T)\kappa(x) \tag{9}$$

It can be seen from Eq. (7), that for thin films the absorption efficiency can be quite small; in fact. as $x \to 0, \kappa \to 0$. This is evident in many thin film "2D materials" where quantum efficiency can be quite poor, and as an illustration, in a single layer graphene, the absorption coefficient is below 3%. In Section 5 below we give a brief description of how thin absorber layers can be used to increase the detector operating temperature.

EQE allows us to calculate the rate of photo-generated carriers. The generation rate can be numerically calculated by:

$$G(T) = \int_0^t \int_0^\infty \eta_{EQE}(\lambda, T, x)n_{opt}(\lambda, T)d\lambda dx \tag{10}$$

Where, $n_{opt}(\lambda, T)$, the photon density can be calculated from Planck's distribution function for a black body source or some other appropriate distribution function for an artificial or structured light source. The generated carrier density is given by $\Delta n = G(T)A_{opt}\tau$ where A_{opt} is the optical area, i.e. the area open to photon collection and generation, and τ is the carrier lifetime. Specific detector design converts this generated carrier density into an equivalent photoresistance, photo-current, or photovoltage which depends on the modality and details of the specific design of the detector. It can be seen that the carrier lifetime plays a critical role; long lived the carrier, better is the signature of photogeneration.

5. Approach to increase the detector operating temperature

As discussed above the photon detector action involves electron-hole pair creation when photons impinge on the absorber layer. Typically, the absorber layer

thickness x requires to be in the order of the wavelength of interest. For example, a 10 μm radiation detection would require at least a 10 μm thick absorber layer. The photons interact in the absorber volume of $A_e x$, where A_e is the electronic area of the detector. Typically, the detector's electronic and optical areas (A_{opt}) are same as shown in **Figure 1a**, and usually denoted as A_d . As shown in **Figure 1b**, the detector absorber layer can be thinned substantially to reduce the absorber volume and thus dark current by using a metastructured stack with optical collection area A_{opt}.

The dark current, which strongly depends on temperature is also proportional to this volume. The total noise current generated in this volume for a noise bandwidth of δf and a gain of g is given as [9]:

$$I_n^2 = 2(G + R)A_e x \delta f q^2 g^2 \tag{11}$$

Where, G and R are the generation and recombination rates and other parameters are defined previously. At equilibrium, $G = R$, and denoted as 2G.

The D^* from Eq. (4) can now be calculated using Eqs. (2) and (3) and yields:

$$D^* = \frac{\eta \lambda}{2hc(xG)^{\frac{1}{2}}} \left(\frac{A_{opt}}{A_e} \right)^{1/2} \tag{12}$$

In Eq. (12) we can see that thickness x is in the denominator. Reducing x will increase D^*, which is what we would want. Another key observation is the ratio of optical collection area to the absorber electronic area. Increasing this ratio also help increase the D^* and thus SNR. However, this can only be true if the quantum efficiency with respect to absorption efficiency $k(x)$ is maintained, see Eq. (9). Thinner x comes at a penalty of lower photon absorption. Therefore, the approach is to reduce the volume by reducing the thickness (x) while maintaining sufficient photon absorption. This can be achieved by the use of a secondary matter particle that is not affected by the thickness and in the contrary prefers a thinned absorber: plasmons. Plasmons [10–12] are collective electromagnetic excitation of the electrons in a material that like to live near the "skin" of the material, characterized by the skin depth δ. The excitation of plasmons by the incident photon then couples with excitonic modes (collectively called polaritons) which can translate into increased electrical response of the material through increased carrier generation that can be detected as increased photocurrent. This approach also yields interesting quantum phenomena such as topologically protected optical behavior, which is not
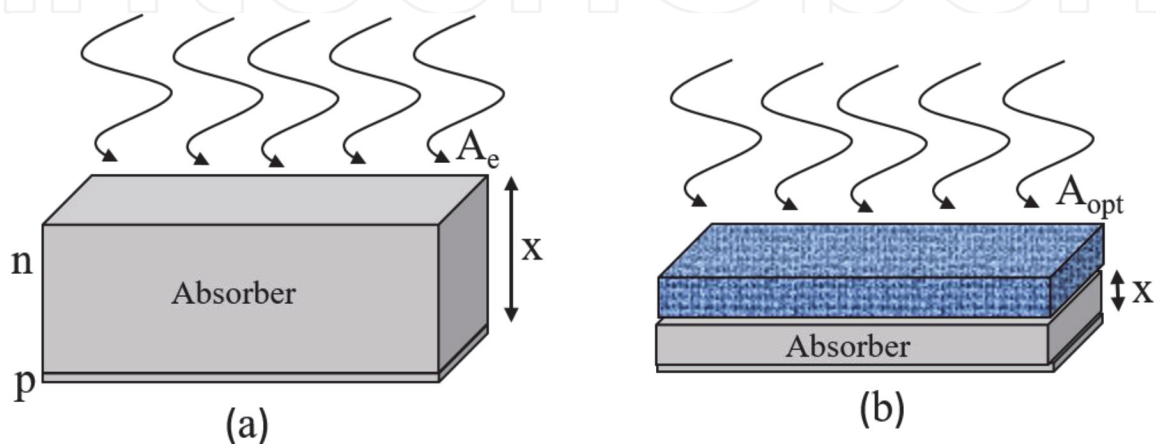

Figure 1.
Illustration of thick (a) and thin (b) design for increasing the detector operating temperature, where A_opt is enhanced absorption using nanostructured materials stack such as metamaterial design.

covered here further. Coupling of photon-plasmon-exciton physics is an exciting field that has led to a whole host of new technologies for detection, including metamaterials [13], negative index materials used in metalenses, and metasurfaces [14–16]. These artificially constructed surfaces (illustrated in **Figure 1b** with area A_{opt}) use carefully designed structure of varying dielectric constants to obtain an artificial composite material that shows behavior not normally seen in any "natural" material. One example of such a material is a matrix of anti-dots, which are voids or physical holes [17, 18] in the detector material that show the physics of absorption enhancement through plasmon polaritons. As shown in **Figure 1b**, the detector absorber volume is reduced considerably and by use of metastructure stack design above one can gain back the photon absorption. More discussions on metastructures is given in Section 9.

6. Leveraging bandstructure engineering for better detectors: artificial materials

Advances in fabrication capabilities at atomic levels, using techniques such as molecular beam epitaxy (MBE), atomic layer deposition (ALD), high precision sputtering and chemical vapor deposition (CVD), and colloidal chemical deposition has brought to us the marvels of building novel materials from ground up; materials such that nature does not build on its own. The use of such materials have proliferated many fields of applied sciences and engineering and new applications come up every few years. In the context of Electrical Engineering, such high precision artificially created nanostructured materials include superlattices, which are candidates for the "next transistor" material. One such example are high mobility GaAs| AlGaAs quantum wells which have been candidates for such devices [19] for a long time, and high electron-mobility transistors (HEMT) [20] built from such quantum wells have proven useful in many applications in telecommunications and low power amplifiers. These composite material stacks are of particular interest due to the tunability of their physical behavior through material design, therefore there is growing interest in such stacks for detector designs. A lot of the recent efforts in exploration of such novel materials have been in lower dimensional materials. Of course, physically every piece of a material has all 3 dimensions; the dimensionality in this context means the physical behavior demonstrated by this material can be captured using condensed matter theories of materials at lower dimensionality. We now briefly discuss the physics that is demonstrated by lower dimensional materials, and discuss the possibilities in sensing applications that have been developed or proposed using such materials.

6.1 Energy levels and 0-D material

First pedagogical problem presented in almost all quantum mechanics text is solving the Schrodinger Equation for a particle in an infinite potential well (i.e. particles cannot leak out from the well) and the resulting quantization of allowed "sharp" energy states which a particle may possess [21]. An immediate extension of this problem in the context of an atom led to the accurate prediction of ionized Hydrogen spectra by Niels Bohr and observation of electron diffraction in Stern-Gerlach experiments, which sealed the deal for quantum mechanics, so to say. The story is more complex in condensed matter where interactions of many electrons in close consort lead to a continuum of allowed states with some gaps in between them. In mid 1980s advances in semiconductor processing allowed fabrication of
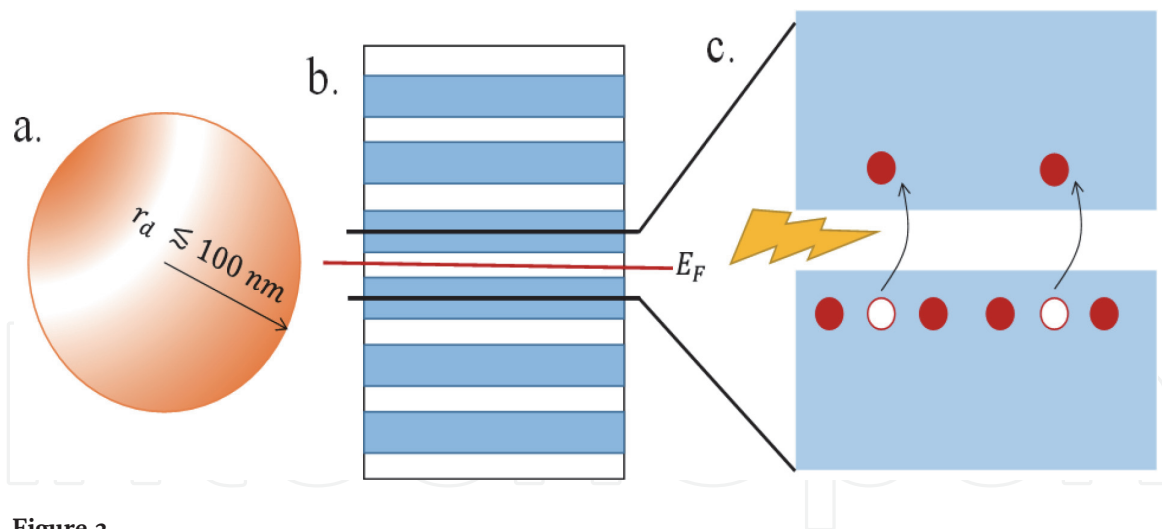
Figure 2.
(a) A quantum dot is made of a semiconducting material with dimensions typically less than 100 nm. (b) The energy spectra of a quantum dot showing a series of thin narrow bands. (c) The two bands of interest: valence and conduction bands participate in photodetection action where incident light promotes electrons from valence to conduction band, from where it can be detected in an external circuitry.

ultra-small dots of particles (**Figure 2a.**) which resemble the pedagogical problem described earlier. The allowed particle states are similarly confined to discrete or very small bands of allowed energies, which are determined primarily by the material type and size of the dots. From the point of view of energy-eigenstates, this is analogous to the particle in a well, only this time it can be physically fabricated with high accuracy and control, hence the name "Quantum Dots" for this kind of a material. It is also immediately obvious why we can call such materials artificial—we can physically select the energy eigenstates rather than depend purely on the intrinsic configuration of the atoms in the material. **Figure 2b** shows an illustrative example of such a material's energy spectra. Ability to tune the eigenstates in quantum dots allows us to build photon detectors of specific wavelength, since the de-Broglie relation links the wavelength to the corresponding energy: $E = \frac{hc}{\lambda}$ where symbols have usual meaning. As an example, the mid-wave infrared (MWIR) corresponds to around 0.25–0.35 eV of energy gaps between conduction and valence bands. Photodetection action then utilizes the light-matter interaction (**Figure 2c**), where incident photon kicks a "bound" electron from valence band to the conduction band which can then be detected -in an external electron counting circuitry.

6.2 From 0-D to 3-D

It is possible to build from bottom-up a picture of evolution of bands and density of states as a function of dimensionality, an illustrative example shown in **Figure 3** (see [21] for a textbook level exposition). Starting from the Gedanken two energy level "simple" model, we obtain a collection of the full 3-D bands. The 0-D can be thought of as a collection of two such bands generally falling on top of each other. However Pauli's Exclusion principle of Fermions do not allow each of these levels to fully overlap, which provides a finite spread of these levels (sub-bands) which are smeared together into a continuum within the bandwidth due to Heisenberg's Uncertainty principle. These two quantum mechanical principles give rise to all bandstructure phenomena in materials.

A 1-D material can be thought of as a collection of multiple 0-D materials, which leads to stacking of multiple thin bands near each other (sub-bands) which merge
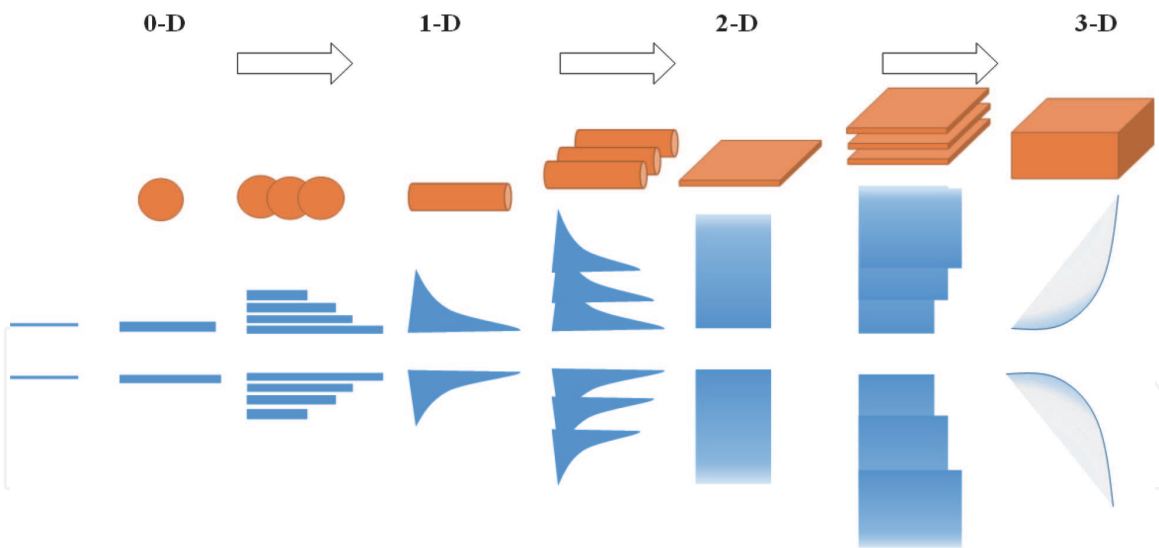
Figure 3.
Evolution of density of states spectra from 0-D sharp bands to 3-D bulk materials.

into a continuous density of states/bands with an energy dependence of $D \propto 1/\sqrt{E}$, this being the density of states of a nanowire. Similarly stacking multiple nanowires together gives us sub-bands that yield into a constant density of states of 2-D materials, prime examples being graphene, MoS_2, black phosphorus etc. Stacking of these 2-D materials then yields the familiar world of 3-D or "bulk" materials with density of states $D \propto \sqrt{E}$.

The advantage of low dimensional materials lie in the density of states and bandstructure that can give rise to unique electrical properties that can be advantageous in building high quality detector. We next discuss some of the engineering opportunities and challenges faced by photodetector materials of low dimensionality.

7. Engineering opportunities and challenges of low dimensionality materials

The current efforts towards building high quality photodetectors are thinned absorbers as discussed before. Lowering the bulk dimensions, particularly the depth, reduce dark current and hence noise. This trend then naturally leads to the exploration of low dimensionality of the material for better detectivity. It should be noted that quantum dots as controlled 0-D materials are popular in photovoltaics and some recent works in IR detectors as well, primarily because of precision in control of detection spectra. Quantum dots are also popular in quantum photonics as coherent photon sources and single spin state storage, and also as detectors of high-frequency shot noise by exploiting transport characteristics in such systems which make them particularly sensitive as detectors. We briefly discuss some of the transport signatures of interest that emerge from low dimensionality.

7.1 Sub-bands and conductance quantum

Confinement in dimensions quantize the corresponding momenta, i.e. the number of "wave modes" of the electrons, similar to confinement of EM waves in waveguides. This can be seen in the intermediate dimension pictures and their corresponding density of states show in **Figure 3**. As discussed before, a 1-D to 2-D

transition shows the signatures of multiple "1-D" density of states pieces coming together to form the 2-D density of states. This can have profound effect on the transport signatures. These discrete transverse modes are activated as a Fermi level crosses through them on the application of an external voltage and the famous "staircase" transmission structure was observed [22] by von Klitzing as integer quantum Hall effect, giving rise to the notion of conductance quantum for each ballistic transmission mode. These signatures can determine the overall current voltage characteristics of a detector structure, which should be considered when a detector structure is designed. These include negative differential resistance or NDR effect, as seen in resonant tunneling diodes. It should be noted that there are further signatures of fractional quantum Hall effects which again arise in ultraclean superlattices at cryogenic temperatures due to topological nature of such Hamiltonians. These states, in particular 2/5 fraction are of great interest for topological quantum computing [23]. It remains to be seen how these two fields can intersect technologically in a meaningful way.

7.2 Contacts

Contacts play a critical role in replenishing and diminishing the carriers in the detector material. This action depends on the relative band alignments between the detector material and the contact. For a low resistance "Ohmic" contact, the corresponding carrier band should be close to each other, since any mismatch leads to resistance as the carriers have to jump "up" or "down", resulting in a change in the momentum and energy, which gives rise to resistance from a mesoscopic point of view [24]. A mismatched contact is called a Schottky contact and works through thermionic emission over the barrier or through a tunneling mechanism. Choice of the contact material plays a critical role in building a high-quality detector, see [25] for a detailed exposition. A low dimensionality material may show narrow bandwidths and low density of states, which do not necessarily make good contacts with bulk wiring leads in a circuit. Choice of a well-matched contact material requires considerable effort. As an example, in quantum dot detectors, the contact is not made directly from the wire lead to the dots themselves, rather they live in a matrix of PMMA and graphite complexes [26]. Recent developments include use of graphene sheets and ribbons to form conformal contacts with the dots and then to a metallic lead. In fact, graphene itself required considerable efforts to find an appropriate contact metal [27]. The central engineering challenge therefore is to build contacts of appropriate quality; in a bipolar structure it may mean building good contacts for both electrons and holes, while in a unipolar, the ideal contact might be an Ohmic one with the transporting carrier, say electron and a blocking Schottky contact with the holes.

7.3 Low density of states

Low dimensional materials often end up showing very low density of states, resulting in low currents even in the case of ultra-low scattering or near ballistic transport. An equivalent analogy of such a case is two cities being connected by a narrow rural one lane road as compared to a four-lane divided highway. The carrying capacity of the former is a bottleneck in transport. This can lead to high shot noise in the material, though cutting down dimensionality may reduce flicker noise due to cutting down of number of possible paths for a carrier to take from one terminal to the other, if the sample is clean. Additionally, 2-D materials may show Anderson localization effect which shows up as an extra resistance in the case of disordered materials, which can then increase and even exceed the flicker noise

seen in bulk samples. It must be noted that while this low current is a critical issue in logic circuits, this is much less of an issue in detectors, and in fact an advantage of low dimension materials by cutting the dark current significantly. However increased noise in disordered materials dictates fabricating high-quality material samples for detector applications.

7.4 Blockaded transport

0 and 1-D materials may show a behavior called the blockaded transport regime. In this regime, due to ultra-low density of states in the material, presence of one electron in the channel "charges up" the channel so much that it prevents another one to enter due to Coulombic repulsion [28]. This is also called the Coulomb blockade. A similar phenomenon can be seen in spin-polarized transport as well, where certain spins are not allowed to go in and out of the channel [29]. Blockaded transport may raise interesting applications for detection since it allows electrical spectroscopy and is a popular method for doing so in STM experiments and molecular electronics [30], though a controlled mechanism for the process will need to be demonstrated before any such application is realized in sensing domain.

7.5 Quantum capacitance

Another consequence of low density of states is the appearance of quantum capacitance in the transport behavior in the material. Quantum capacitance is given as $C_q = q^2 D$ [31]. It can be seen that as the density of states D goes down, the capacitance goes down. This capacitance then effects the electrostatics and transient behavior of the detector material with consequences for detector design and operation. As per basic circuit laws, series capacitances add up as harmonic sum, which is dominated by the smallest capacitance in the system. For large bulk systems, C_q is substantial and can be ignored in device capacitance considerations, however in nanowires or nanosheets it starts to play a substantial role. Central consequence of this phenomena is diminished control over the detector electrostatics, particularly if the detector is working in photoFET mode. Therefore, it is critical to design a detector keeping in consideration of quantum capacitance in low dimensions.

8. Modeling and simulation approaches for nanostructures: quantum effects, light-matter interaction, carrier transport

Modeling approaches in nanostructures can be roughly divided into three categories of techniques, dealing with the different particles that come into picture in the detector physics. We broadly divide the discussion into bosonic and fermionic particles, as their physics are very different and therefore their modeling approaches have differed in their developments. It is impossible to cover all these myriad approaches in a single volume monolog, much less in a section of a chapter, therefore we provide only a very brief overview of these approaches along with some textbook references that can serve as starting point for deeper education and understanding.

For "bosonic" particles such as photons, plasmons (and various associated polaritons), phonons etc. it is customary to use a wavelike approach i.e. by solving a wave equation in a classical physics sense [32], and it is rarely necessary to approach them with quantum field theoretic approaches, i.e. second quantization methods. Photons are indeed extremely well modeled using a classical Lagrangian written by

formalizing the Maxwell's equation in terms of a 4-vector gauge theory [33]. Similar approaches work very well for plasmons, which are the collective oscillations of electrons, or phonons which are mechanical oscillations of the material lattice. Both plasmons and phonons show a dispersion relation, i.e. an energy-momentum relation with similar structure (optical and acoustic branches) and therefore are amenable to a unified approach to modeling and simulations.

This above fact is exploited by the many available computational electromagnetics software that convert the wave equation, which is a vector PDE boundary value problem into a linear algebra problem using the technique of Finite Element Analysis (FEA). This approach converts a physical domain into a collection of packed small triangular (most widely used shape in FEA) regions over which the solution is considered to be constant. In one iteration the solution over the "finite elements" are updated based on the previous step values, and this iteration continues till the error value over the whole grid reaches a minimum threshold, set as per the specifications of the problem. See [34] for a classic text on FEA. Other similar approaches include finite difference method, which instead of creating a mesh of triangles that can cover any possible physical geometry, uses a Cartesian grid on which the derivatives are discretized over "grid points" instead of triangular regions as used in FEA, and the problem is converted into a linear algebra problem. An associated method called the finite volume method (FVM) generalizes FEA and FEM to 3D problems. However these approaches are general enough that they can be extended to any dimensions, with associated approaches to discretization. The relative "mechanistic" approach of these methods that depend on linear algebraic methods have allowed development of extremely power simulators, including Ansys HFSS, COMSOL Multi-Physics, MATLAB etc. which can now utilize GPUs to accelerate the solution of very large problems.

For "fermionic" particles such as electrons and holes, the approaches differ in the sets of equations which are solved, depending on the application. Traditionally Boltzmann transport equation (BTE) has been a popular method in solving electron transport problems. However powerful many-body quantum statistical mechanics approaches have been developed as well, the central one being the Non-Equilibrium Green's Function (NEGF) method that has shown tremendous success in solving the problem of electron transport in complex material stacks such as superlattices and nanostructures. A classic exposition that covers both these approaches in an extremely approachable way is [35]. We next describe the fundamental principles underlying these methods and their application spaces.

The central entity of the Boltzman transport equation is the carrier distribution function $f(t, p, q)$ which is a function of time t, generalized position p, associated momentum q. The equation can be written as:

$$\dot{f} + \dot{p}\nabla_p f + \dot{q}\nabla_q f = Sf \tag{13}$$

Where ∇f denotes the gradient of f with respect to the subscripted variable, S is a scattering operator that mixes the distribution function in various p and q states, depending on the particular problem being addressed. In general solving this problem for even one particle involves keeping track of the distribution function in a 7D phase-space (6D in a steady state problem), which can quickly become intractable for even moderate sized problems, especially interacting systems. Therefore, the most commonly used approach to solve this PDE is to use Monte Carlo methods which allows us to construct the full solution by evaluating only certain trajectories through the phase-space, instead of calculating the full phase-space. Careful application of importance sampling can lead to fast tractable solutions to f from which it is possible to then calculate current-voltage relations (first moment), noise currents

(second moment), and even higher order moments as necessary. It is possible to also calculate heat flows by energy weighted first moment of f.

NEGF method can be seen as a quantum analog of Boltzman transport equation. The central quantity of the interest in this formalism are the retarded Green's function G^r, which the "causal" propagator of the carrier in the system, and the correlation function $G^<$ which is the quantum density matrix. The NEGF method evolves the $G^<$ under the influence of various scattering phenomena (Büttiker probes are a good example) under the action of the G^r. The two equations are written as:

$$G^r = [E - H - \Sigma]^{-1} \tag{14}$$

$$-iG^< = G^r \Sigma^{in} G^a \tag{15}$$

Where E is the energy, H is the system Hamiltonian, Σ is the total "self energy" for all the scattering mechanisms applicable to the system, including physical contacts, momentum scattering, dephasing, inelastic scattering etc. Σ^{in} is the corresponding sum of the "inflows" from these mechanisms into the system. We leave the details of how these may be written to the reference mentioned above and other follow on works from the author, a recognized authority on the subject.

The NEGF approach is well suited to handle any arbitrary combinations of material stacks, i.e. an arbitrary H, not necessarily confined to materials with parabolic bands. This method also forgoes any equilibrium or near equilibrium assumption that is commonly applied in BTE. Transport phenomena of lower dimensional, and indeed any quantum system is automatically incorporated in the NEGF approach. This makes NEGF a very powerful tool for modern detector structures which are increasingly based on superlattices. However, incorporating appropriate self-energy and inflow terms in the NEGF equation requires a non-trivial intellectual effort. As the field develops further we expect phenomena such as Auger recombination, Impact ionization, SRH recombination, multi-electron generation etc. will be included systematically in the toolset of NEGF methods, which will then yield a truly bottom-up quantum mechanical simulation approach for photonic devices.

9. Metasurfaces for LWIR devices

In this section, we now explore the possibility of exploiting the fast-developing area of metasurfaces—more generally known as flat optics—to add functionality to the existing IR sensors without affecting the performance or increasing SWaP. In addition, metasurfaces offer a possibility of increasing the temperature of operation. In reference to **Figure 1b**, the metasurface-coupled detector is an emerging technology to enhance optical absorption in a thin detector architecture. This becomes even more important where absorber layer is naturally thin—such as quantum dots, 2D materials— or require to be thin bulk absorber to minimize dark current and overall detector materials noise.

As the electromagnetic radiation passes through a resonant element, both its amplitude and phase undergo a large change. Interestingly the phase can be varied from 0 to π either for the frequencies in the vicinity of the resonant frequency as shown in **Figure 4** or equivalently for element size in the vicinity of size that is resonant at a given frequency. Particularly the latter observation along with little or no variation in amplitude can be exploited to introduce phase variation in the XY-plane (for the light propagating in Z direction) of the optoelectronic device. With
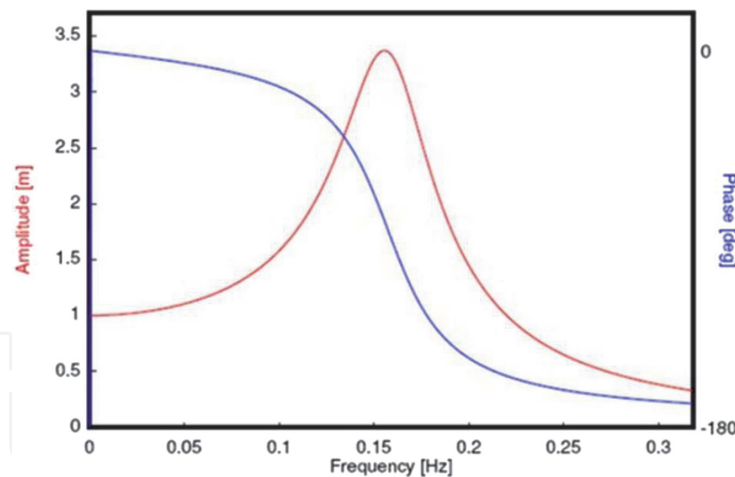
Figure 4.
Schematic variation in amplitude (red) and phase (blue) near the resonant frequency of the metaelement.

appropriate phase gradient on a dielectric surface—called metasurface—and the generalized Fresnel's equations [36, 37], we can change the propagation wave front to arbitrary shape and direction, leading to a number of interesting applications [36, 37].

Interestingly, the functions such as focusing, defocusing, total reflection, total transmission, total absorption, frequency filtering, non-specular reflection and/or transmission, polarization filtering, which often requires bulky optical elements, can be achieved with sub-wavelength-thick metasurface [38–44]. The metaelements include sub-wavelength and appropriately shaped metal—known as plasmonics—and all-dielectric, size-dependent Mie resonant scatterer. The advantage of metal plasmonics is that the size can be exceedingly small (often 1/10th of the wavelength) and field concentration/redirection can be huge. However, ohmic loss in metals often affects the optical absorption required in the optical devices. On the other hand, Mie resonant scatterer with a transparent dielectric can provide required phase change without any absorption but requires high index contrast for efficient light modulation. Since the Mie element size is $\sim \lambda/n$ (where λ is the design wavelength and n is refractive index of the dielectric) for resonance, the metasurface unit cell can contain only a few elements and hence a broadband design is often difficult. For illustration, we consider three applications—near-perfect reflection [42, 43] polarization filter [44] and broadband absorption [45, 46] for possible high temperature operation.

Our work in metasurface area is motivated by adding functionalities and operability to the existing IR devices. For example, a metasurface for near-perfect narrow band reflection. Highly reflective surfaces are of great interest for several applications, including sensor and eye protection under laser illumination, hardware hardening against laser irradiation, and optical elements in high-energy laser systems. In these applications, the surfaces require high reflectivity under intense illumination with little or no absorption or transmission. To protect the IR device from the high intensity radiation at a wavelength in the absorbing band, an ultrathin metasurface can be fabricated on the optical devices and the elements of the metasurface can be chosen to fully reflect the high intensity wavelength. We have used shape-dependent Mie scattering to design ultra-thin metasurfaces and demonstrated [43] near-perfect reflection (>99.5%) in a narrow band (around 1550 nm) as shown in **Figure 5**. Note that $\sim$500 nm-tall Si nanopillars (with index 3.5) on low index SiO_2 (index 1.45) are sufficient to achieve the high reflection without any metal component. The design principle is applicable to all reflection windows with appropriate changes to the element size and materials set.
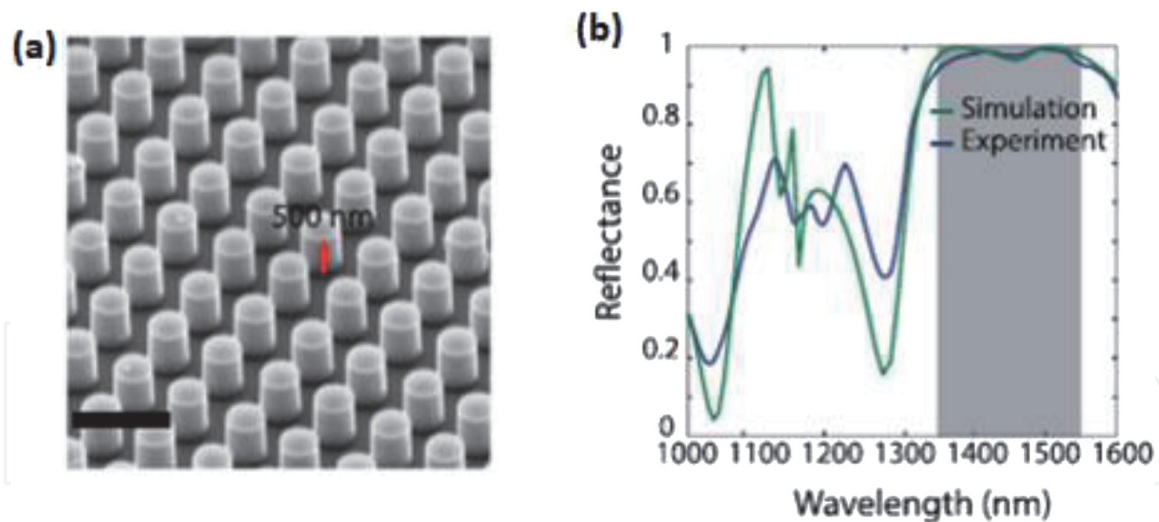
Figure 5.
(a) Fabricated Si nanopillars on SiO$_2$ and (b) the simulated (green) and measured (black) reflectance [43].

The constituent materials for short-wavelength infrared to the long-wavelength infrared, can be, for example Si, InP, or GaAs for the high index and ZnS, BaF$_2$, CaF$_2$, or MgF$_2$ for the low index materials that have high transparency with little or no absorption to 12 μm.

The polarization of the radiation can be exploited to improve imaging quality, particularly when the thermal contrast between a target and its background is insufficient for polarization-insensitive sensors [47]. Two kinds of polarizers—absorptive polarizers and polarization beam splitters—are currently used. Absorptive polarizers such as wire grids, dichroic materials, or nanoparticle composites provide high degrees of polarization, but both polarizations cannot be analyzed simultaneously as needed in applications such as imaging and quantum information. The polarization beam splitters such as birefringent cubes or Brewster angle reflection in multilayer dielectric films preserve the rejected polarization by reflection or diffraction. However, they are bulky for chip-scale photonic and optoelectronic devices. We have slightly modified the design of **Figure 5** to introduce lattice asymmetry as shown in **Figure 6a** so that resonance frequency for S- and P-polarizations are separated. Consequently, one polarization is reflected nearperfectly while the other is transmitted near totally as demonstrated (**Figure 6b**). The small difference in the transmitted component between simulations (dashed) and measured (solid) are because of over-etching of SiO$_2$ around the pillars which can be corrected. Notice that mere 500 nm-thick metasurface, which can be monolithically integrated with the sensor can provide near perfect polarization splitting to add polarimetric functionality to the existing IR devices. The concept can be extended to other wavelength bands with appropriate choice of transparent materials. As can be noted, the reflectivity changes in a narrow band and the structures are useful in applications where the large bandwidth is not a requirement. However, several options including the optimization in height to diameter ratio, periodicity of the pillars, multiple element with differing size in the unit cell are available to increase the bandwidth.

Metasurfaces for broadband absorption and transmission will be more useful in IR sensors in increasing the operating temperature. We discuss the issues limiting the temperature of operations and then some metasurface designs that offer the possibility of addressing these issues.

Sensing technology in the infrared (IR) spectrum enables substantial advances in several applications including security, surveillance, industrial monitoring, and
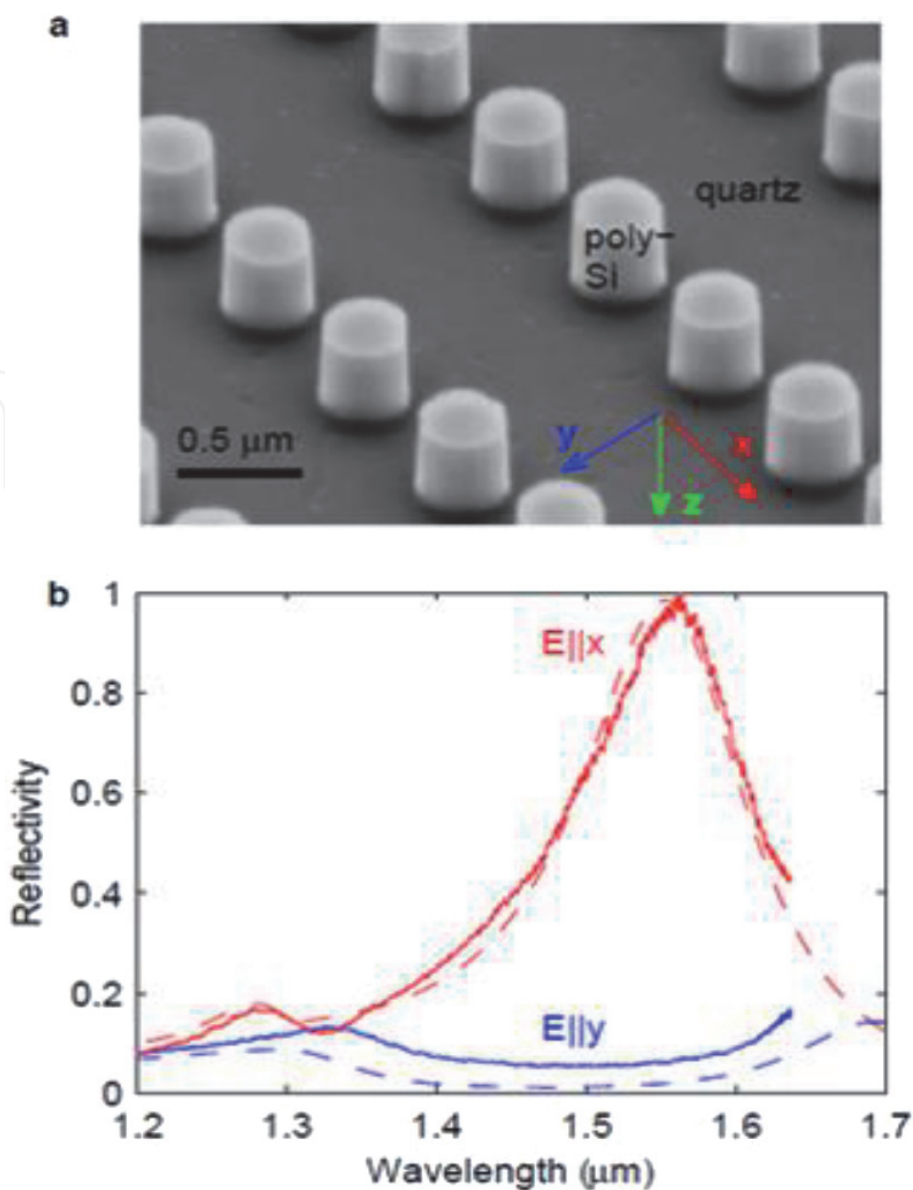
Figure 6.
(a) Fabricated Si nanopillars on SiO₂ and (b) the simulated (dashed) and measured (solid) polarization-dependent reflectance [44].

autonomous vehicle navigation. The reduction in SWaP of these sensors without sacrificing performance is particularly important. Among various IR technologies, long wavelength infrared (LWIR) imaging systems are crucial for target-acquisition tasks because of their advantages in adverse environments. Current detection and imaging technologies that cover the LWIR spectral regions typically operate at cryogenic temperatures of 77 K or lower. This requires expensive and bulky cooling systems that increase the overall SWaP of imagers. Uncooled LWIR detector would greatly alleviate the SWaP constraint and enhance the imaging system's portability, enabling broad applications in surveillance and reconnaissance under adverse conditions.

The increase in operating temperatures often requires unfavorable tradeoff between performance, cost, and power consumption. In photon detectors, the dark current increases exponentially with temperature as depicted in Eq. (6), resulting in more power consumption, high noise, deeper cooling requirements and thus poorer performance. Uncooled microbolometers for imaging have a considerably lower performance as compared to cooled photodetectors. Novel and nanocrystalline materials such as colloidal quantum dots (CQDs) show promise, but the synthesis of large sized particles for absorption in the LWIR with fewer surface states needs to

be mastered. There is a large number of publications [48, 49] demonstrating LWIR sensing at room temperature with 2D materials—often exploiting high absorption in thin layers and the Schottky barrier between them and Si—and also by measuring the changing properties resulting from high absorption in structured graphene [50], for example. While these results are encouraging, considerable improvements are needed to increase the QE—because only carriers within a few nm from the interface participate in absorption—and the path forward for integrating with ROICs for imaging is not clear.

For many years, there has been a continuing effort to increase the operating temperatures (T_d) of IR detectors and arrays with conventional materials such as HgCdTe and type II superlattices (T2SL). The efforts include high-quality materials to reduce defect-mediated dark currents, low n-doping to achieve high depletion and suppress Auger and radiative-mediated dark currents, strained layer superlattices to reduce the Auger mediated dark currents, novel device architectures such as nBn and CBIRD, and others to reduce the diffusion currents, as well as optical immersion lenses, photon trapping structures, and plasmonic structures to reduce the collection volume and thus dark currents. However, the epitaxial layers of LWIR photodetectors are still very thick, requiring long growth times and creating sensitivity to chamber and source maintenance, inevitably promoting the numbers of SRH centers. Beyond some critical photodetector thickness, dark current begins to dominate and the signal-to-noise ratio of a photodetector decreases.

Current LWIR sensors employing p-n junctions require absorbers with a thickness equal to or greater than the targeted cut off wavelength (~12 μm-thick for LWIR) for ~80% absorption of the incident radiation [51]. However, as mentioned before, the thick absorption region results in a large dark current, arising from generation mediated by the Auger, radiative and Shockley-Read-Hall (SRH) mechanisms [52]. Efforts to reduce the dark current via higher bias (for depletion) increases the band-to-band and/or trap-assisted tunneling and thus do not offer a robust solution [53]. For example, higher depletion by very low doping of LWIR detectors did not increase the operating temperatures beyond 100 K [54]. Various prior efforts to pattern the entry surface—known as photon trapping or PT structures— succeeded in minimizing Fresnel reflection but achieved only a moderate decrease in absorption region thickness and a slight increase in operating temperature of larger band gap mid-wavelength infrared (MWIR) devices to near 200 K [55–57]. Since the absorption in the structured surface did not increase the photocurrent, the overall QE actually becomes poorer.

Recently, LWIR and MWIR photodetectors based on T2SLs, especially Ga-free ones, have shown promising performance [58]. However, the LWIR operation temperature is still limited to 77 K [59]. GaSb-based T2SLs have a higher operation temperature, but the temperature increase (up to 110 K) is still modest for a 10-μm cut-off [60]. In addition, epitaxially grown quantum dots (QDs), which are sometimes coupled with quantum wells, have been used to increase the operation temperature up to 200 K [61]. The challenge of epitaxial QDs lies in their low QE. CQDs have shown promise in the MWIR with a high QE. Still, the dark current and noise are high owing to their poor transport properties [62]. The requirements for high temperature of operation are illustrated [63] in **Figure 7**. The assumptions in this illustrative calculation include—8–10 μm spectral band, *f*/1 optics, 10 μm detector cut off, 70% in-band QE and 19 Me-integrated charge (30 Me-well). We note that when the absorber thickness *t* is 10 μm, the lowest noise equivalent differential temperature (NEdT) of 30 mK (red) is above the preferred value of 20 mK. When the collection volume is reduced *without loss* of QE (blue), we can increase T_d by about 20–40 K. However, when this reduction in volume is combined with Auger suppression by a factor of 50, for example expected in superlattices because of flat
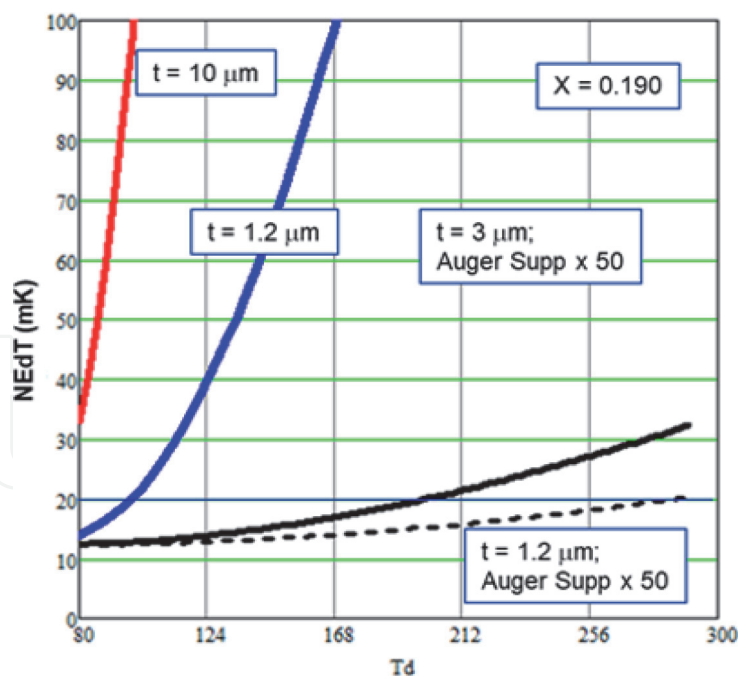
Figure 7.
Effect of collection volume and auger on detector performance [63].

bands or in a lightly depleted absorber, the T_d can be increased (dotted) to ~270 K. More specifically, the designs for high temperature operation should meet the following criteria:

1. Large reduction in collection volume *without loss* of QE.

2. Full depletion at lower bias.

3. Reduction in minority carrier leakage current.

Having examined the aforementioned efforts of improving the operation temperature of LWIR photodetectors, we conclude that any approach to increase the operating temperature will require a substantial reduction in absorption thickness as we know thinner absorber reduces the collection volume, is easier to fully deplete with small voltages, and result in few defect centers.

The resonant pixel approach [64] developed by Choi et al. attempts to reduce the collection volume by allowing the light to enter through thin metallic layer and force it to go through multiple reflection by sandwiching the absorber between two metal layers. This effort has been successful, for example, in reducing the absorber thickness to 0.7–1.2 μm and still achieve quantum efficiency of 50–70% with about 2 μm bandwidth in LWIR region [63, 65]. The use of metal, required for resonant cavity, causes ohmic loss and further increase in bandwidth and quantum efficiency have not yet been demonstrated.

Several metasurfaces are proposed or demonstrated to achieve broadband absorption. However most of them use metallic elements, limiting the absorption in the dielectric absorber layer which cannot increase the photocurrent, and are not considered here. We will discuss two promising all-dielectric designs [45, 46]. To enable high absorption for solar application with thin MoS_2 layers, the authors [45] proposed a structure shown in **Figure 8a** with corresponding absorption measurements shown in **Figure 8b**. Although this structure resembles that of Fabry-Perot cavity structure, they designed a photonic band gap (PBG) in standoff oxide layer to increase the absorption in MoS_2 through increasing the interaction with guided
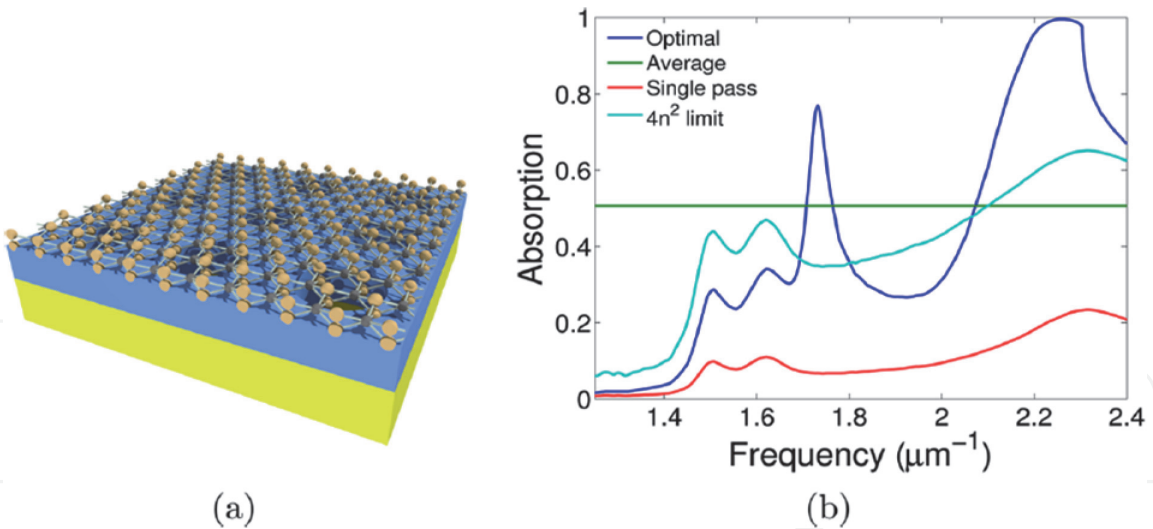
Figure 8.
(a) Modified Fabry-Perot structure to include a photonic band gap design (periodic holes) in the oxide layer and (b) the predicted absorption spectrum (blue) in the monolayer MoS$_2$ [45].

resonance of the PBG. With a single layer MoS$_2$ (of thickness ~0.6 nm) and an absorption coefficient of ~2×10^5 cm^{-1}, a broadband average of 50% absorption in the visible is predicted. The scalable design can be extended to mid- and long-wave infrared region and even with 100× smaller absorption coefficient, the absorber thickness can be estimated to be ~65 nm for this level of absorption. However, a detailed modeling absorption dispersion in the LWIR band is required to ensure that guided mode traverses through the entire absorber thickness required for even higher QE.

Interestingly, broadband all-dielectric transmitting metasurface—in the visible band—has been demonstrated [46]. Appropriately designed Si nanopillars on Si absorber (**Figure 9a**) has been fabricated (**Figure 9b**) and reflectance has been measured to be very low and broad band (**Figure 9c**, black). All the rest are transmitted and absorbed in Si. Notice that absorption is on the average over 95% broadband covering entire visible spectrum. The nanopillars behave like anantenna funneling the radiation over larger area, covering the nanopillar and the surrounding metal in the unit, through the pillars into the absorbing substrate. The funneling effect increases the electric field right below the nanopillars, resulting in absorption
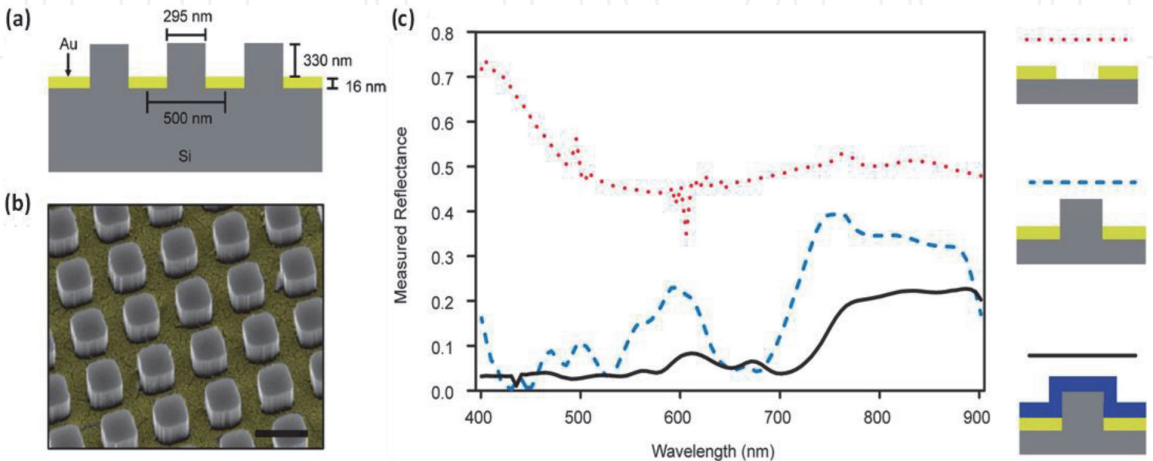

Figure 9.
(a) Cross section of the absorber (si) with metasurface (b) fabricated metasurface, and (c) measured reflectance without absorbing nanopillar (red), with absorbing nano pillar (blue) and with antireflection coated (black) [46].
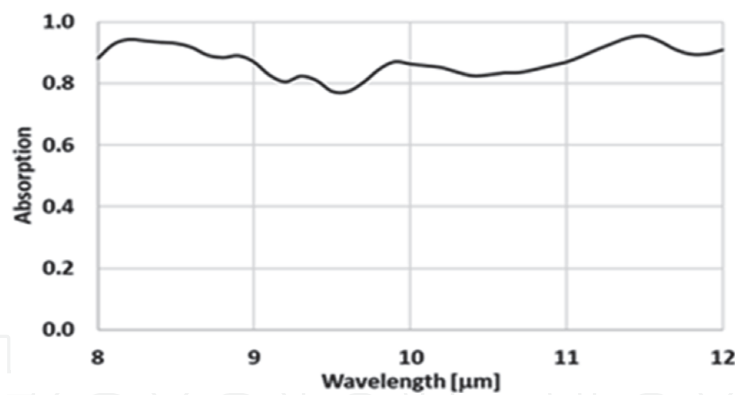
Figure 10.
Predicted absorption spectrum in 2 μm-thick absorber with a metasurface.

enhancement in this layers. Note another important consequence of the funneling effect is that radiation does not impinge on the metal, allowing the metasurface to be transparent and conduction. This feature is particularly very important for all electrically operated IR devices.

Noting that above design is scalable, we have designed a similar structure with appropriate choice of materials for LWIR and the calculated absorption spectrum with 2 μm-thick absorber is shown in **Figure 10**. We see that about 80% broadband absorption is possible. Absorber without the metasurface will require to be at least 12 μm thick to achieve this level of absorption. In essence, the absorber volume can be reduced by a minimum of 6-fold reducing the dark current proportionately. Further, 2 μm low doped region is far easier to fully deplete, resulting in considerable reduction in Auger scattering, which further reduces the dark currents. Also, smaller bias is sufficient to achieve depletion, reducing the power consumption. The device development is in progress for possible 300 K operation.

10. Summary

In summary, the fast-developing field of metasurfaces show considerable promise for easier integration with the detector absorber layer to both, increase the SWAP performance and the operating temperature. This chapter discussed various approaches to using nanostructured metasurface designs to increase the photon capture by enhancing the apparent collection area A_{opt} while decreasing the electronic absorption volume, $A_e x$. We discussed from ground-up the physics of the photodetection as an interplay of energy transfer from light to matter particles, which may take many routes, which all contribute to the large phase space of photodetector design. We discussed why there is a need for development of ultra-thin and even lower dimensional materials for photodetection, to cut down on dark current and the corresponding decrease in the noise. This allows us to trade D^* enhancements with higher operating temperatures. We discussed the implications on the light absorption of ultra-thin and low dimensional materials, compared to their bulk counterparts. We also discussed some unique transport signatures that are enabled at low dimensions, including quantized conductance, reduction of flicker noise in ultra-clean 2D materials. We also mentioned issues of material integration and electrical controllability due to contact physics and quantum of capacitance. We briefly discussed the numerical approaches taken for simulation of photonic and electronic components. We provided a detailed exposition of the physics of metasurfaces to bring back the quantum efficiency in ultra-thin and low

dimensional detectors. We further discussed the increasing trend of using bandstructure engineering (T2SL) in building detectors, in particular nBn and complementary barrier detectors which engineer the electron transport properties of the detector, and how even such "novel" materials benefit from thinness of the detector material in achieving high operating temperature.

We hope that in this chapter we have provided a broad overview of the rich physics of photodetectors to the reader and provided further points to ponder over and references to follow for more in-depth education. The future prospects of infrared detectors are clearly in the direction of nanostructure designs to develop, not only systems that eliminates bulky cryogenic coolers, but also looks into thin sensor architectures that can be conformal. In addition, there will be a significant advancement in the area of focal plane array and readout electronic designs with subsequent system designs that will push intelligence near the sensor. The emergence of Artificial Intelligence, Machine Learning and neuromorphic approaches will also drive more and more functionalities in the sensor that will reduce the data pipeline, post processing and lag associated with current technologies.

Author details

Nibir Kumar Dhar[1*], Samiran Ganguly[2] and Srini Krishnamurthy[3]

1 Virginia Commonwealth University, Richmond, VA, USA

2 University of Virginia, Charlottesville, VA, USA

3 Sivananthan Laboratories, Bolingbrook, IL, USA

*Address all correspondence to: dharnk@vcu.edu

IntechOpen

References

[1] Dhar NK et al. Optoelectronics—Advanced Materials and Devices. Rijeka: IntechOpen; 2013 (Chapter 7)

[2] Kinch MA. Tutorial Texts in Optical Engineering. Vol. TT76. Bellingham, WA: SPIE Press; 2007

[3] Palaferri D et al. Ultra-subwavelength resonators for high temperature high performance quantum detectors. New Journal of Physics. 2016;**18**:113016

[4] Rogalski A. Infrared Detectors. CRC Press; 2010

[5] Ganguly S et al. A multiscale materials-to-systems modeling of polycrystalline PbSe photodetectors. Journal of Applied Physics. 2019;**126**(14):143103

[6] Shockley W, Queisser HJ. Detailed balance limit of efficiency of p-n junction solar cells. Journal of Applied Physics. 1961;**32**:510

[7] Moss TS. Photoconductivity. Reports on Progress in Physics. 1965;**28**:15

[8] Urbach F. The long-wavelength edge of photographic sensitivity and of the electronic absorption of solids. Physics Review. 1953;**92**:1324

[9] Martyniuk P et al. HOT infrared photodetectors. Opto-Electronics Review. 2013;**21**(2):239-257

[10] Zayats AV, Smolyaninov II, Maradudin AA. Nano-optics of surface plasmon polaritons. Physics Reports. 2005;**408**(3-4):131-314

[11] Pitarke JM, Silkin VM, Chulkov EV, Echenique PM. Theory of surface plasmons and surface-plasmon polaritons. Reports on Progress in Physics. 2006;**70**(1):1

[12] Ditlbacher H, Krenn JR, Schider G, Leitner A, Aussenegg FR. Two-dimensional optics with surface plasmon polaritons. Applied Physics Letters. 2002;**81**(10):1762-1764

[13] Cai W, Shalaev VM. Optical Metamaterials. Vol. 10(6011). New York: Springer; 2010

[14] Choi K-K, Dutta A, Dhar N. Novel IR photodetectors and energy harvesting devices. IEEE Journal of Quantum Electronics. 2021;**1172303**

[15] Grayer J, Ganguly S, Yoo S-S. Plasmonics: Design, Materials, Fabrication, Characterization, and Applications XVII. Vol. 11082. San Diego, CA: International Society for Optics and Photonics; 2019

[16] Holloway CL, Kuester EF, Gordon JA, O'Hara J, Booth J, Smith DR. An overview of the theory and applications of metasurfaces. IEEE Antennas and Propagation Magazine. 2012;**54**(2):10-35

[17] Rabiee-Golgir H et al. Infrared Technology and Applications XLV. Vol. 11002. Baltimore, MD: International Society for Optics and Photonics; 2019

[18] Safaei A et al. Wide angle dynamically tunable enhanced infrared absorption on large-area nanopatterned graphene. ACS Nano. 2018;**13**(1):421-428

[19] Shur MS. GaAs Devices and Circuits. Berlin/Heidelberg, Germany: Springer Science & Business Media; 2013

[20] Smith, P. M., et al. 1987 IEEE MTT-S International Microwave Symposium Digest. Vol. 2. Las Vegas, NV: IEEE; 1987.

[21] Ghosh A. Nanoelectronics: A Molecular View. Singapore: World Scientific; 2016

[22] Klitzing KV, Dorda G, Pepper M. New method for high-accuracy determination of the fine-structure constant based on quantized hall resistance. Physical Review Letters. 1980;**45**(6):494-497

[23] An S, Jiang P, Choi H, Kang W, Simon SH, Pfeiffer LN. arXiv:1112.3400

[24] Datta S. Lessons from Nanoelectronics: A New Perspective on Transport. Vol. 1. World Scientific Publishing Co Inc; 2012

[25] Ganguly S, Yoo S-S. On the choice of metallic contacts with polycrystalline PbSe films and its effect on carrier sweepout and performance in MWIR detectors. Journal of Electronic Materials. 2019;**48**(10):6169-6175

[26] Zheng W, Wong S-C. Electrical conductivity and dielectric properties of PMMA/expanded graphite composites. Composites Science and Technology. 2003;**63**(2):225-235

[27] Xia F et al. The origins and limits of metal-graphene junction resistance. Nature Nanotechnology. 2011;**6**(3): 179-184

[28] Muralidharan B et al. Theory of high bias coulomb blockade in ultrashort molecules. IEEE Transactions on Nanotechnology. 2007; **6**(5):536-544

[29] Muralidharan B, Datta S. Generic model for current collapse in spin-blockaded transport. Physical Review B. 2007;**76**(3):035432

[30] Dorogi M et al. Room-temperature Coulomb blockade from a self-assembled molecular nanostructure. Physical Review B. 1995;**52**(12):9071

[31] Guo J et al. Electrostatics of nanowire transistors. IEEE Transactions on Nanotechnology. 2003; **2**(4):329-334

[32] John David Jackson. Classic Electrodynamics. 3rd ed. New York: Wiley; 1999

[33] Hehl F, Obukhov Y. Foundations of Classical Electrodynamics. Basel, Switzerland: Birkhäuser; 2003

[34] Thomas JR. Hughes: The Finite Element Method: Linear Static and Dynamic Finite Element Analysis. Hoboken, NJ: Prentice-Hall; 1987

[35] Datta S. Electronic Transport in Mesoscopic Systems. Cambridge, UK: Cambridge University Press; 1997

[36] Yu N et al. Light propagation with phase discontinuities: Generalized laws of reflection and refraction. Science. 2011;**334**:333-337

[37] Aieta F et al. Out-of-plane reflection and refraction of light by anisotropic optical antenna metasurfaces with phase discontinuities. Nano Letters. 2012;**12**: 1702-1706

[38] Glybovski SB et al. Metasurfaces: From microwaves to visible. Physics Reports. 2016;**634**:1

[39] Jung J et al. Broadband metamaterials and metasurfaces: A review from the perspectives of materials and devices. Nanophotonics. 2020;**9**:3165-3196

[40] Arbabi A et al. Dielectric metasurfaces for complete control of phase and polarization with subwavelength spatial resolution and high transmission. Nature Nanotechnology. 2015;**10**:937

[41] Khorasaninejad M et al. Efficient polarization beam splitter pixels based on a dielectric metasurface. Optica. 2015;**2**:376

[42] Slovick B, Yu ZG, Berding M, Krishnamurthy S. Perfect dielectric-metamaterial reflector. Physical Review B. 2013;**88**:165116

[43] Moitra P et al. Experimental demonstration of a broadband all-dielectric metamaterial perfect reflector. Applied Physics Letters. 2014;**104**:171102

[44] Slovick B, Zhou Y, Yu ZG, Kravchenko I, Briggs D, Moitra P, et al. Metasurface polarization splitter. Philosophical Transactions of the Royal Society A. 2017;**375**:20160072

[45] Piper JR, Fan S. Broadband absorption enhancement in solar cells with an atomically thin active layer. ACS Photonics. 2016;**3**:571

[46] Narasimhan et al. Hybrid metalsemiconductor nanostructure for ultrahigh optical absorption and low electrical resistance at optoelectronic interfaces. ACS Nano. 2015;**9**:10590

[47] Tyo JS, Goldstein DL, Chenault DB, Shaw JA. Review of passive imaging polarimetry for remote sensing applications. Applied Optics. 2006;**45**(22):5453-5469

[48] Lan C et al. 2D materials beyond graphene towards Si integrated infrared optoelectronics devices. Nanoscale. 2020;**12**:11784 and the references cited therein

[49] Long M et al. PdSe$_2$ long wavelength infrared photodetector with high sensitivity and stability. ACS Nano. 2019;**13**:2511

[50] Safaei S, Chanda D. Dynamically tunable extraordinary light absorption in monolayer graphene. Physical Review B. 2017;**96**:165431

[51] Lee D et al. High operating temperature HgCdTe: a vision for the near future. Journal of Electronic Materials. 2016;**45**:4587

[52] For the latest review see, Rogalski A. HgCdTe Photodetectors, Mid-infrared Optoelectronics. Amsterdam, Netherlands: Elsevier; 2020 (Ch. 7)

[53] Krishnamurthy et al. Tunneling in LWIR Photodiodes. Journal of Electronic Materials. 2006;**35**:1399

[54] Strong RL et al. Performance of 12-μm- to 15-μm-pitch MWIR and LWIR HgCdTe FPAs at elevated temperatures. Journal of Electronic Materials. 2013;**42**:3103

[55] Martynuik P et al. New concepts in infrared photodetector designs. Applied Physics Reviews. 2014;**1**:041102

[56] Choi KK et al. Resonant structures for IR photodetection. Applied Optics B. 2017;**56**:1559

[57] Choi KK. Metastructures for VLWIR SLS detectors. In: Proc. SPIE 11407, IR Tech. and Applications XLVI, 114070K. Anaheim, CA: SPIE; 2020

[58] Haddadi A et al. Bias–selectable nBn dual–band long−/very long−wavelength infrared photodetectors based on InAs/InAs1- xSbx/AlAs1- xSb x type–II superlattices. Scientific Reports. 2017;**7**:3379

[59] Nguyen BM, Hoffman D, Huang EKW, Delaunay PY, Razeghi M. Background limited long wavelength infrared type-II InAs/GaSb superlattice photodiodes operating at 110 K. Applied Physics Letters. 2008;**93**:123502

[60] Pour SA et al. High operating temperature midwave infrared photodiodes and focal plane arrays based on type-II InAs/GaSb superlattices. Applied Physics Letters. 2011;**98**:143501

[61] Yamanaka T et al. Gain-length scaling in quantum dot/quantum well infrared photodetectors. Applied Physics Letters. 2009;**95**:093502

[62] Lhuillier E, Guyot-Sionnest P. Recent progresses in mid infrared nanocrystal optoelectronics. IEEE

Journal of Selected Topics in Quantum
Electronics. 2017;**23**:1-8

[63] Velichu S. Private communication

[64] Choi KK et al. Resonator-quantum
well infrared photodetectors. Applied
Physics Letters. 2013;**103**:201113

[65] Choi KK et al. Small pitch resonator-
QWIP detectors and arrays. Infrared
Physics and Technology. 2018;**94**:118